

Article

# Nonlinear Dynamics of Exclusive Excited-State Emission Quantum Dot Lasers Under Optical Injection

Zai-Fu Jiang <sup>1,2</sup>, Zheng-Mao Wu <sup>1,\*</sup>, Elumalai Jayaprasath <sup>1</sup>, Wen-Yan Yang <sup>1,3</sup>,  
Chun-Xia Hu <sup>1,4</sup> and Guang-Qiong Xia <sup>1,\*</sup>

<sup>1</sup> School of Physical Science and Technology, Southwest University, Chongqing 400715, China; jiangzaifu23003@163.com (Z.-F.J.); ejayaprasath@gmail.com (E.J.); swyangwy@163.com (W.-Y.Y.); huxiaoxia101@126.com (C.-X.H.)

<sup>2</sup> School of Mathematics and Physics, Jingchu University of Technology, Jingmen 448000, China

<sup>3</sup> School of Physics, Chongqing University of Science and Technology, Chongqing 401331, China

<sup>4</sup> College of Mobile Telecommunications, Chongqing University of Posts and Telecom, Chongqing 401520, China

\* Correspondence: zmwu@swu.edu.cn (Z.-M.W.); gqxia@swu.edu.cn (G.-Q.X.)

Received: 28 April 2019; Accepted: 23 May 2019; Published: 27 May 2019



**Abstract:** We numerically investigate the nonlinear dynamic properties of an exclusive excited-state (ES) emission quantum dot (QD) laser under optical injection. The results show that, under suitable injection parameters, the ES-QD laser can exhibit rich nonlinear dynamical behaviors, such as injection locking (IL), period one (P1), period two (P2), multi-period (MP), and chaotic pulsation (CP). Through mapping these dynamic states in the parameter space of the frequency detuning and the injection coefficient, it can be found that the IL occupies a wide region and the dynamic evolution routes appear in multiple forms. Via permutation entropy (PE) calculation to quantify the complexity of the CP state, the parameter range for acquiring the chaos with high complexity can be determined. Moreover, the influence of the linewidth enhancement factor (LEF) on the dynamical state of the ES-QD laser is analyzed. With the increase of the LEF value, the chaotic area shrinks (expands) in the negative (positive) frequency detuning region, and the IL region gradually shifts towards the negative frequency detuning.

**Keywords:** quantum dot lasers; excited-state; nonlinear dynamics; optical injection

## 1. Introduction

Under external perturbations, semiconductor lasers (SLs) can exhibit various nonlinear dynamical behaviors, such as the period one (P1), period two (P2), multi-period (MP), and chaos (CO) etc. [1–5], which has attracted much attention due to their potential applications in photonic microwave amplifiers [6], optical frequency converters [7], wireless optical fiber communication [8], all-optical logic gates [9], laser Doppler velocimeters [10], secure optical communication, and random bit generation [11–13].

Among different types of SLs, a self-organized SL with quantum dot (QD) structure has turned out to be very promising [14–17] due to such unique properties as low relative intensity noise [18], a small linewidth enhancement factor (LEF) [19,20], and high temperature stability [21]. For the QD lasers, three-dimensional quantum confinement gives rise to discrete energy levels for electrons and holes. Under a relatively low bias current, the recombination of electrons and holes in the ground-state (GS) results in sole GS emission. As the bias current is increased, the population of the excited-state (ES) increases. When the current exceeds the secondary threshold, the QD lasers simultaneously emit

in both the GS and the ES. Moreover, when the bias current is high enough, the QD lasers may emit solely in the ES [22]. In recent years, the nonlinear dynamics of the QD lasers subject to external perturbations have received considerable attention [23–29]. For a QD laser emitting solely in the GS, Erneux et al. have theoretically and experimentally investigated its dynamic response under optical injection, and the results show that the laser has similar dynamic features to the Class A laser [23]. Goulding et al. have reported the excitability after introducing optical injection, and the excitable pulses and the random conversion between the stable and unstable states were observed [24]. Carroll et al. have experimentally studied the instabilities resulted by optical feedback and the irregular power drop-outs and the periodic pulsations are presented [25]. For the case of a QD laser simultaneously emitting in the GS and the ES, Viktorov et al. have reported the low-frequency inverse phase fluctuation phenomenon of the ES and GS lasing intensities caused by optical feedback [26]. Olejniczak et al. have theoretically demonstrated that the ES lasing intensity shows regular picosecond pulses and pulse packages when the wavelength of injection light is close to the lasing wavelength of the GS mode [27]. For a QD laser emitting solely in the ES under high bias currents, a tunable all-optical gating has been implemented after introducing optical injection [28], and the hysteresis phenomenon has also been observed by scanning the injection power along different variation routes [29].

Recently, relevant investigations demonstrated that, through adopting some special techniques during the manufacture, QD lasers can emit exclusively in the ES [30–32], named as ES-QD lasers in this work. Different from ordinary QD lasers, such ES-QD lasers always emit in the ES while the GS is suppressed totally [30]. Compared with ordinary QD lasers, ES-QD lasers possess higher differential gain, a smaller relaxation oscillation (RO) damping rate, and a smaller K-factor [30,31], which are helpful for enhancing the modulation response and the nonlinear dynamical properties [30–35]. The modulation speeds of ES-QD lasers can reach 25 Gbps (on-off keying (OOK)) and 35 Gbps (pulse-amplitude modulation (PAM)) [30,32]. Meanwhile, ES-QD lasers possess broad modulation bandwidths and low chirp-to-power ratios [33]. In addition, through introducing optical feedback, diverse nonlinear dynamic states, such as the periodic and chaotic states, have been observed in the ES-QD lasers [34,35]. Besides the modulation and optical feedback, optical injection is another frequently used external perturbation technique. We have noted that related research on the nonlinear dynamics of ES-QD lasers under optical injection is rarely reported. In this work, based on a theoretical model of ES-QD lasers [33,36–38], after taking into account optical injection, the nonlinear dynamics of ES-QD lasers under optical injection are investigated. The mapping of the dynamical states in the parameter space of frequency detuning and the injection coefficient is presented, and the effect of the linewidth enhancement factor (LEF) on the nonlinear dynamics of ES-QD lasers is also discussed.

## 2. Theoretical Model

A schematic diagram of the carrier dynamics for ES-QD lasers is shown in Figure 1. Here, charged electrons and holes are regarded as the neutral excitons (electron-hole pairs), and the differences among QDs are neglected, i.e., there is only one QD ensemble in the active region [38]. By electric pumping, the carriers are directly pumped into the reservoir (RS) plane. Through Auger processes, some carriers are captured from RS to ES during the time of  $\tau_{ES}^{RS}$ , and then some carriers relax from ES to GS during the time of  $\tau_{GS}^{ES}$  [37]. Additionally, due to the thermal excitations, some carriers in GS (ES) escape to ES (RS) during the time of  $\tau_{ES}^{GS}$  ( $\tau_{RS}^{ES}$ ) [37]. It is assumed that the system is in quasi-equilibrium and the carrier number in each energy level satisfies the Fermi–Dirac distribution. It is worth noting that this model ignores the direct carrier capture path from RS to GS. The stimulated radiation can occur in ES or GS for ordinary QD lasers, but only the ES lases in the ES-QD lasers [33]. After referring to References [33,36–38] and taking optical injection into account, the rate equations for optical injection ES-QD lasers can be described by the following:

$$\frac{dN_{RS}}{dt} = \frac{\eta I}{e} + \frac{N_{ES}}{\tau_{RS}^{ES}} - \frac{N_{RS}}{\tau_{ES}^{RS}}(1 - \rho_{ES}) - \frac{N_{RS}}{\tau_{RS}^{spont}}, \quad (1)$$

$$\frac{dN_{ES}}{dt} = \left( \frac{N_{RS}}{\tau_{RS}} + \frac{N_{GS}}{\tau_{ES}} \right) (1 - \rho_{ES}) - \frac{N_{ES}}{\tau_{RS}} - \frac{N_{ES}}{\tau_{GS}} (1 - \rho_{GS}) - \frac{N_{ES}}{\tau_{ES}^{spont}} - \Gamma_p v_g g_{ES} S, \quad (2)$$

$$\frac{dN_{GS}}{dt} = \frac{N_{ES}}{\tau_{GS}} (1 - \rho_{GS}) - \frac{N_{GS}}{\tau_{ES}} (1 - \rho_{ES}) - \frac{N_{GS}}{\tau_{GS}^{spont}}, \quad (3)$$

$$\frac{dS}{dt} = \left( \Gamma_p v_g g_{ES} - \frac{1}{\tau_p} \right) S + \beta_{sp} \frac{N_{ES}}{\tau_{ES}^{spont}} + \frac{2K}{\tau_{in}} \sqrt{S_0 S} \cos(2\pi\Delta\nu t - \phi), \quad (4)$$

$$\frac{d\phi}{dt} = \frac{1}{2} \alpha \left( \Gamma_p v_g g_{ES} - \frac{1}{\tau_p} \right) + \frac{K}{\tau_{in}} \sqrt{\frac{S_0}{S}} \sin(2\pi\Delta\nu t - \phi), \quad (5)$$

where abbreviations *RS*, *ES*, and *GS* stand for the reservoir, the excited-state, and the ground-state, respectively, and superscript *spont* represents the spontaneous emission. The value *N* denotes the carrier number, *S* is the photon number, and  $\phi$  is the electric field phase. The value *I* denotes the bias current,  $\eta$  represents the current pumping efficiency, and *e* represents the elementary charge of an electron. The value  $\Gamma_p$  denotes the optical confinement factor. The values  $\tau_p$  and  $\tau^{spont}$  represent the photon lifetime and the spontaneous decay time, respectively. The value  $v_g$  is the group velocity of light, and  $\tau_{in}$  is the round-trip time of light in a cavity of length *L*. The terms  $\rho_{GS}$  ( $=N_{GS}/2N_B$ ) and  $\rho_{ES}$  ( $=N_{ES}/4N_B$ ) represent the occupancy probabilities of carriers in GS and ES, where  $N_B$  denotes the total QD number. The terms  $1 - \rho_{GS}$  and  $1 - \rho_{ES}$  are the Pauli-blocking factors [38,39], which correspond to the probabilities of empty QD state in GS and ES. The value  $S_0$  is the photon number of the free-running ES-QD laser. The value *K* is the injection coefficient and  $\Delta\nu$  represents the frequency detuning between the injection light and the free-running ES-QD laser. The gain coefficient,  $g_{ES}$ , of ES is expressed as follows:

$$g_{ES} = \frac{a_{ES}}{1 + \xi \frac{S}{V_S}} \frac{N_B}{V_B} (2\rho_{ES} - 1), \quad (6)$$

where  $a_{ES}$  denotes the differential gain of ES,  $\xi$  represents the gain limiting factor,  $V_B$  is the total volume of QDs, and  $V_S$  denotes the intra-cavity laser field volume.

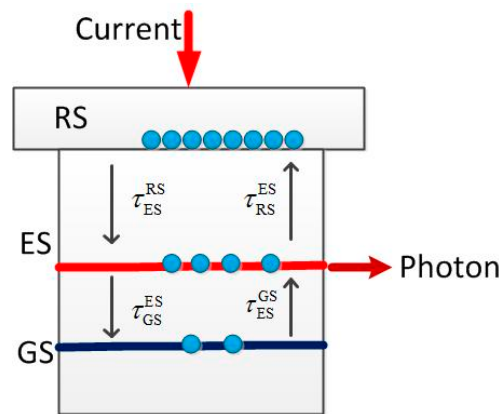


**Figure 1.** Schematic diagram of the carrier dynamics for the ES-QD lasers. GS: ground-state; ES: excited-state; RS: reservoir.

Numerical methods for the solution of ordinary differential equations are the main tools to investigate the nonlinear dynamical systems [40,41]. In this work, a desktop PC with a six-core processor (AMD Ryzen 5 1600X, Advanced Micro Devices Inc., Santa Clara, CA, USA) and 16GB installed memory is used to perform the simulation, and we adopt the ode45 solver (Fourth-Fifth order Runge–Kutta algorithm, where the fourth-order provides the candidate solutions and the fifth-order controls the errors) in MATLAB software to solve the above differential equations, after taking into account the accuracy and speed of the calculations. Since the step size will affect the simulation

results [40], we use the adaptive step size in numerical simulations. The used parameters for the ES-QD laser during the simulations are given in Table 1 [33,38].

**Table 1.** Simulation parameters of the QD laser.

Symbol	Parameter	Value
$E_{RS}$	RS recombination energy	0.97 eV
$E_{ES}$	ES recombination energy	0.87 eV
$E_{GS}$	GS recombination energy	0.82 eV
$\tau_{ES}^{RS}$	Capture time from RS to ES	12.6 ps
$\tau_{ES}^{ES}$	Relaxation time from ES to GS	5.8 ps
$\tau_{ES}^{GS}$	Escape time from ES to RS	5.4 ns
$\tau_{GS}^{ES}$	Escape time from GS to ES	20.8 ps
$\tau_{RS}^{ES}$	RS spontaneous decay time	0.5 ns
$\tau_{ES}^{ES}$	ES spontaneous decay time	0.5 ns
$\tau_{GS}^{ES}$	GS spontaneous decay time	1.2 ns
$\tau_p$	The lifetime of photon	4.1 ps
$L$	Cavity length	$5 \times 10^{-2}$ cm
$a_{ES}$	Differential gain of ES	$10 \times 10^{-15}$ cm <sup>2</sup>
$\xi$	Gain limiting factor	$2 \times 10^{-16}$ cm <sup>2</sup>
$\Gamma_p$	Optical confinement factor	0.06
$N_B$	Total QD number	$1 \times 10^7$
$\alpha$	Linewidth enhancement factor	1.3
$v_g$	Group velocity of light	$8.57 \times 10^7$ m/s
$V_B$	Total volume of QDs	$5 \times 10^{-11}$ cm <sup>3</sup>
$\eta$	Current pumping efficiency	0.15

### 3. Results and Discussion

Figure 2a shows the power-current ( $P$ - $I$ ) curve of the free-running ES-QD laser. Obviously, the threshold current ( $I_{th}$ ) of the laser is about 92.0 mA. As the current increased from 92.0 mA to 250.0 mA, the output power increased linearly. Figure 2b displays the variations of the carrier number in ES and GS with the current. From this diagram, it can be seen that the carrier numbers in ES and GS are almost constant for the laser biased above the threshold, and the former is larger since the degeneracy of ES is twice that of GS [33]. Furthermore, by using small signal analysis, the relaxation oscillation (RO) frequencies of the ES-QD laser at different bias currents can be obtained, as shown in Figure 2c. With the increase of the current, the RO frequency increases nonlinearly. In the following discussion, the current of the laser is fixed at  $I = 184.0$  mA ( $= 2I_{th}$ ) and the corresponding RO frequency is about 7.60 GHz.

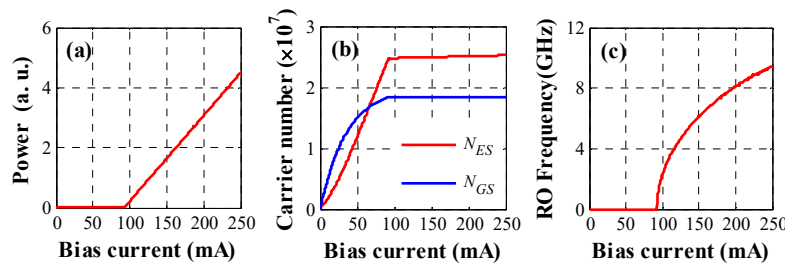


**Figure 2.** Output power (a), carrier number (b), and relaxation oscillation (RO) frequency (c) of the ES-QD laser as a function of the bias current.

Our simulations demonstrate that after introducing an optical injection, the ES-QD laser can exhibit different dynamical states. Figure 3 shows the time series, power spectra, and phase portraits of the ES-QD laser, under optical injection with frequency detuning  $\Delta\nu = -14.00$  GHz and different injection coefficient  $K$ . For  $K = 0.30$  (Figure 3a1–a3), the time series behaves as a periodic oscillation whose

fundamental frequency is about 14.26 GHz, which can be captured from the power spectrum, and the trajectories of phase portrait show a clear limit cycle feature. As a result, it can be determined that the ES-QD laser operates at the period one (P1) oscillation. For  $K = 0.33$  (Figure 3b1–b3), the periodic waveform with two peak intensities can be clearly observed in the time series, the sub-harmonic frequency (about 7.13 GHz) appears in the power spectrum, and the corresponding phase portrait possesses two loops that are intertwined together. Under this case, the ES-QD laser exhibits the period two (P2) oscillation. For  $K = 0.49$  (Figure 3c1–c3), multiple peaks with different intensities emerge in the time series, multiple new frequency components appear upon the power spectrum, and the phase portrait shows the overlap alternation of multiple loops. Therefore, the dynamics of the ES-QD laser can be judged as the multi-period (MP) state. For  $K = 0.64$  (Figure 3d1–d3), the peak intensity of the time series behaves as an irregular fluctuation, the associated power spectrum broadens, and the phase portrait exhibits a strange attractor. Based on these features, the dynamic state of the ES-QD laser can be determined to be the chaotic pulsation (CP) state. When  $K$  is increased to 0.90 (Figure 3e1–e3), the time series shows a stable output, no obvious peak can be observed in the power spectrum, and the corresponding phase portrait shows a stable point. Further calculation shows that, under this condition, the lasing frequency of the ES-QD laser is just the frequency of the injection light. As a result, it can be judged that the ES-QD laser operates at the injection locking (IL) state.

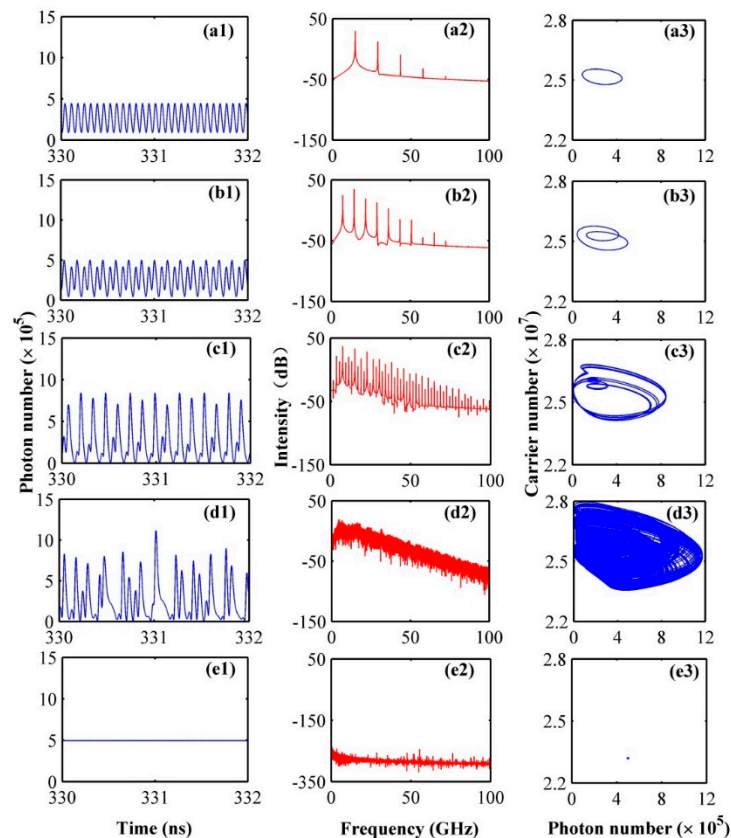


**Figure 3.** Time series (first column), power spectra (second column), and phase portraits (third column) of the ES-QD laser for  $\Delta\nu = -14.00$  GHz and different  $K$ , where  $K = 0.30$  (a1–a3),  $K = 0.33$  (b1–b3),  $K = 0.49$  (c1–c3),  $K = 0.64$  (d1–d3), and  $K = 0.90$  (e1–e3).

Figure 4 shows a bifurcation diagram for observing the dynamical evolution of the ES-QD laser with the injection coefficient  $K$  at  $\Delta\nu = -14.00$  GHz. As shown in this diagram, when the injection coefficient  $K$  increases from 0 to 0.32, the output waveform has two extreme values and the ES-QD laser can be judged to operate at the period one (P1) oscillation. When the injection coefficient  $K$  increases from 0.32 to 0.47, the output waveform has four extreme values and the laser can be determined to be

the period two (P2) oscillation. Further increasing the injection coefficient  $K$  from 0.47 to 1, the ES-QD laser presents the multi-period (MP), the chaotic pulsation (CP), and the injection locking (IL).

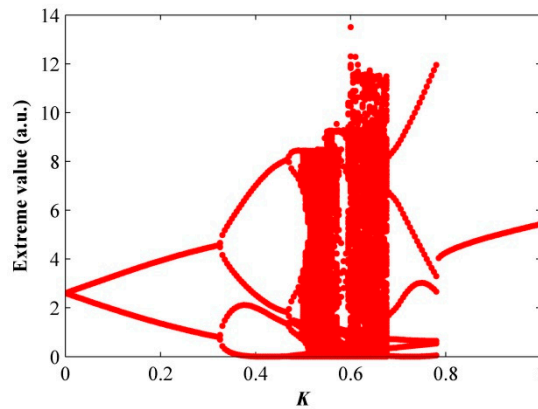


Figure 4. Bifurcation diagrams of the ES-QD laser for  $\Delta\nu = -14.00$  GHz.

The above results are obtained under different  $K$  for a fixed  $\Delta\nu = -14.00$  GHz. Next, in order to understand the nonlinear dynamical evolution of the ES-QD laser more comprehensively, a mapping of the dynamic states in the parameter space of  $K$  and  $\Delta\nu$  is presented in Figure 5a, where different colors represent different dynamical states. As shown in this diagram, some dynamic states including injection locking (IL), period one (P1), period two (P2), multi-period (MP), and chaotic pulsation (CP) can be observed for the ES-QD laser, under different injection parameters. It is worth noting that a large area of IL appears in the map due to optical injection. In the positive frequency detuning region, around  $\Delta\nu = 4.00$  GHz, the P1-P2-MP-IL dynamic evolution is exhibited with the increase of the injection coefficient, but the CP does not emerge. In the negative detuning region, around  $\Delta\nu = -4.00$  GHz and  $\Delta\nu = -14.00$  GHz, the typical dynamic evolutions of P1-P2-IL and P1-P2-MP-CP-MP-IL are presented with the increase of the injection coefficient, respectively. It can be seen that the ES-QD laser, under optical injection, can output abundantly dynamical states and exhibit multiple forms of dynamic evolution routes. In addition, we have noticed that the CP state mainly exists in the regions of  $0.48 < K < 0.68$  and  $-15.00 \text{ GHz} < \Delta\nu < -13.00 \text{ GHz}$ . In order to further explore the characteristics of the CP state, we have calculated the normalized permutation entropy (PE),  $h_s$ , to quantify the complexity of the CP signal, and the PE is defined as follows [42,43]. The time series  $\{S(m), m = 1, 2, \dots, N\}$  are firstly reconstructed into a set of  $D$ -dimensional vectors after choosing an appropriate embedding dimension  $D$ , and then we study all  $D!$  permutation  $\pi$  of order  $D$ . For each  $\pi$ , the relative frequency (# means number) is determined as follows:

$$p(\pi) = \frac{\#\{m|m \leq N - D, (S_{m+1}, \dots, S_{m+D}) \text{ has type } \pi\}}{N - D + 1}. \tag{7}$$

The PE is given by

$$h[p] = -\sum p(\pi) \log(p(\pi)). \tag{8}$$

Then, the normalized PE is further defined as follows:

$$h_s = \frac{h[p]}{h_{\max}} = \frac{-\sum p(\pi) \log(p(\pi))}{\log(D!)}, \tag{9}$$

where  $h_s = 0$  and  $h_s = 1$  represent a completely predictable process and a completely stochastic process with uniform probability distribution, respectively. We use a 670 ns length of the time series and the embedding dimension  $D = 6$  to calculate the PE. Figure 5b displays the complexity of the CP in the parameter space of  $K$  and  $\Delta\nu$ , where different colors represent different complexity values. From this

diagram, it can be observed that the CP state with a high complexity of  $0.95 < h_s < 0.98$  is mainly located at the regions of  $0.55 < K < 0.67$  and  $-14.50 \text{ GHz} < \Delta\nu < -13.30 \text{ GHz}$ .

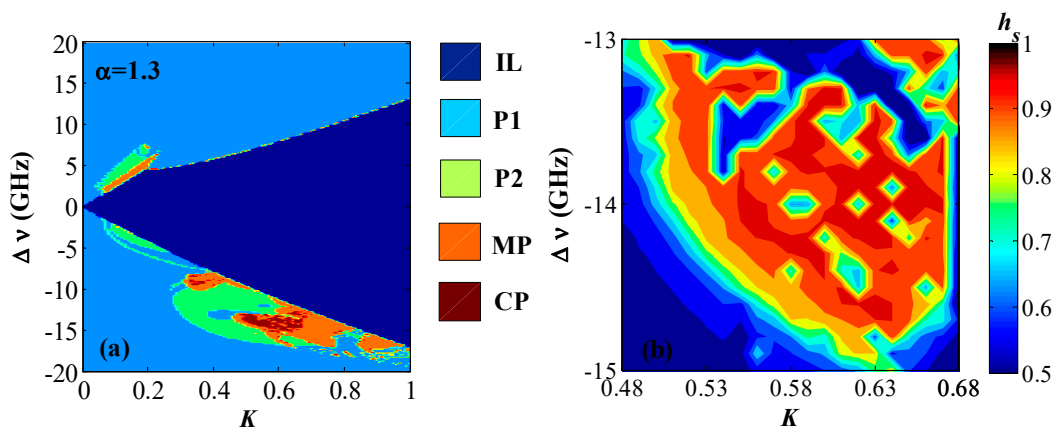


**Figure 5.** (a) Nonlinear dynamics distribution and (b) corresponding chaotic region complexity distribution of the ES-QD laser in the parameter space of injection coefficient and frequency detuning. IL: injection locking, P1: period one, P2: period two, MP: multi-period, CP: chaotic pulsation.

It is well known that the linewidth enhancement factor (LEF) is one of key parameters that affects the spectral linewidth, the mode stability, as well as the nonlinear dynamics of SLs under external perturbations [44–46]. The above results were obtained under a fixed LEF value of 1.3. In Reference [33], it is pointed out that the differential gain of each energy level and the energy separation between resonant and non-resonant states will have a profound impact on the LEF value. As a result, it is necessary to investigate the effect of the LEF on the nonlinear dynamics of ES-QD lasers. Figure 6 shows the mappings of the nonlinear dynamic behaviors in the parameter space of  $\Delta\nu$  and  $K$  under different  $\alpha$ . For  $\alpha = 0.5$  (Figure 6a), in the region of  $\Delta\nu > 0$ , the injection locking (IL), period one (P1), period two (P2), and multi-period (MP) can be observed, while in the region of  $\Delta\nu < 0$ , besides IL, P1, P2, and MP, a chaotic pulsation (CP) region (brown) can be found nearby ( $\Delta\nu = -10.00 \text{ GHz}$ ,  $K = 0.45$ ), and is surrounded by the MP state. Additionally, as shown in this diagram, the stable IL region (dark blue) almost symmetrically distributes in both sides of  $\Delta\nu = 0$ . For  $\alpha = 1.0, 1.5$  (Figure 6b,c), with the increase of the LEF value, the area of the P2 region (light green) increases significantly, the IL region slowly moves towards the range of  $\Delta\nu < 0$ , and the CP region shifts to nearby ( $\Delta\nu = -15.00 \text{ GHz}$ ,  $K = 0.6$ ). For  $\alpha = 2.0, 2.5$ , and  $3.0$  (Figure 6d–f), as the LEF value increases, the IL region gradually shifts to the negative detuning side and asymmetrically distributes in both sides of  $\Delta\nu = 0$ , but its area is approximately unchanged. In addition, the area of the CP region gradually expands (shrinks) in the range of  $\Delta\nu > 0$  ( $\Delta\nu < 0$ ), and finally predominantly distributes nearby ( $\Delta\nu = 6.00 \text{ GHz}$ ,  $K = 0.25$ ). Moreover, the area of the P2 region is approximately unchanged and the area of the MP region (orange) gradually shrinks. It can be seen that the change of LEF value profoundly affects the dynamic distribution of the ES-QD laser under optical injection.

In addition, it should be pointed out that the classical Fourth-Fifth order Runge–Kutta method is used for numerical simulation in this work. Relevant research shows that different numerical simulation methods will affect the discrete behavior of nonlinear systems and may obtain different results [41]. As a result, we will concern and verify the validity of different numerical simulation methods by combining experimental observations in our next research.

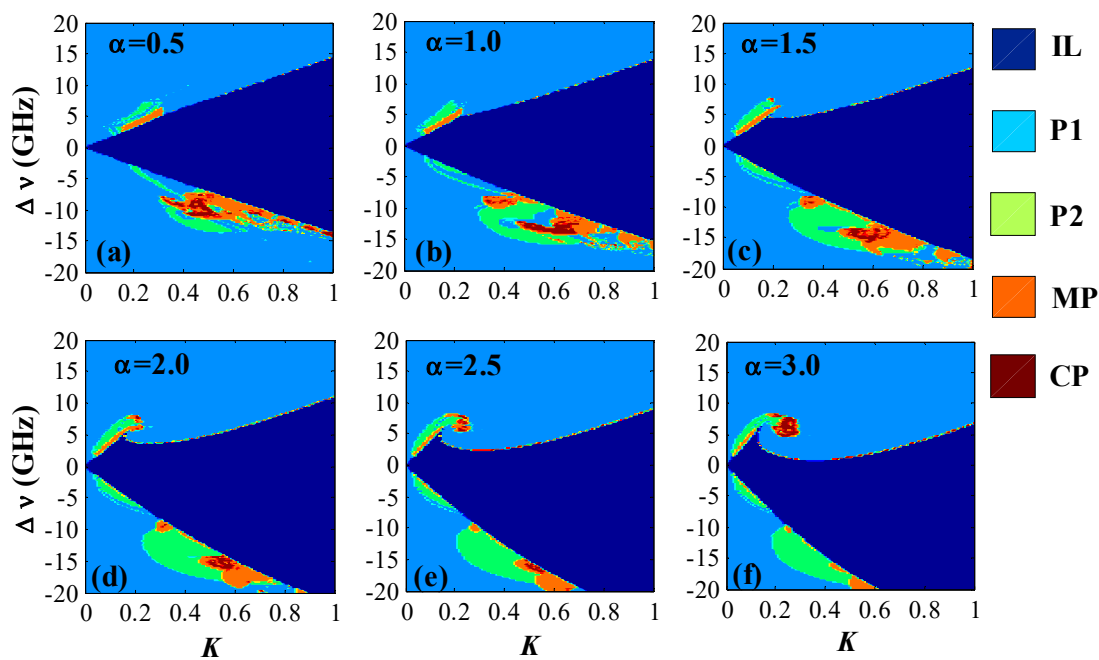


**Figure 6.** Mappings of the nonlinear dynamics distribution of the ES-QD Laser in the parameter space of injection strength and frequency detuning for different LEF, where (a)  $\alpha = 0.5$ , (b)  $\alpha = 1.0$ , (c)  $\alpha = 1.5$ , (d)  $\alpha = 2.0$ , (e)  $\alpha = 2.5$ , and (f)  $\alpha = 3.0$ . IL: injection locking, P1: period one, P2: period two, MP: multi-period, CP: chaotic pulsation.

#### 4. Conclusions

In summary, the nonlinear dynamics of an exclusive ES emission QD laser under optical injection have been investigated numerically. The results show that, under suitable optical injection parameters, the ES-QD laser can exhibit a series of nonlinear dynamical behaviors such as injection locking (IL), period one (P1), period two (P2), multi-period (MP) and chaotic pulsation (CP). Through mapping these dynamic states in the parameter space of  $\Delta\nu$  and  $K$ , the typical dynamic evolution routes of P1-P2-IL, P1-P2-MP-IL, and P1-P2-MP-CP-MP-IL are observed. The IL region has a large area and the CP is mainly distributed in the regions of  $0.48 < K < 0.68$  and  $-15.00 \text{ GHz} < \Delta\nu < -13.00 \text{ GHz}$ . Through the PE calculation to quantify the complexity of CP state, the CP with a high complexity  $0.95 < h_s < 0.98$  is located at the regions of  $0.55 < K < 0.67$  and  $-14.50 \text{ GHz} < \Delta\nu < -13.30 \text{ GHz}$ . In addition, the influence of the linewidth enhancement factor (LEF) on the dynamic behavior distributions of the ES-QD laser is also discussed. With the increase of the LEF value, the CP region moves to the positive frequency detuning range and distributes nearby ( $\Delta\nu = 6.00 \text{ GHz}$ ,  $K = 0.25$ ), the area of the MP gradually shrinks, and the IL region gradually shifts to the negative frequency detuning range and its area is approximately unchanged. Compared with the dynamical characteristics of distributed feedback (DFB) lasers under optical injection, the dynamical evolutionary trends are similar, but the chaotic region of DFB lasers is larger and the IL region for DFB lasers will gradually disappear with the increase of LEF [45]. These differences may be due to the three-dimensional restriction of carriers in QD lasers. We believe that this work would be helpful for understanding the nonlinear dynamics of ES-QD lasers under optical injection and then exploiting related applications.

**Author Contributions:** Z.-F.J. was responsible for the numerical simulation, analyzing the results, and the writing of the paper. E.J., W.-Y.Y. and C.-X.H. were responsible for writing and revising the manuscript. Z.-M.W. and G.-Q.X. were responsible for the discussion of the results and reviewing/editing/proof-reading of the manuscript.

**Funding:** This research was funded by the National Natural Science Foundation of China (Grant Nos. 61475127, 61575163, 61775184, and 61875167).

**Conflicts of Interest:** The authors declare no conflict of interest.

## References

1. Yan, S.L. Period-control and chaos-anti-control of a semiconductor laser using the twisted fiber. *Chin. Phys. B* **2016**, *25*, 090504. [[CrossRef](#)]
2. Chen, J.J.; Duan, Y.N.; Li, L.F.; Zhong, Z.Q. Wideband polarization-resolved chaos with time-delay signature suppression in VCSELs subject to dual chaotic optical injections. *IEEE Access* **2018**, *6*, 66807–66815. [[CrossRef](#)]
3. Hohl, A.; Gavrielides, A. Bifurcation cascade in a semiconductor laser subject to optical feedback. *Phys. Rev. Lett.* **1999**, *82*, 1148–1151. [[CrossRef](#)]
4. Lin, F.Y.; Liu, J.M. Harmonic frequency locking in a semiconductor laser with delayed negative optoelectronic feedback. *Appl. Phys. Lett.* **2002**, *81*, 3128–3130. [[CrossRef](#)]
5. Zhang, M.J.; Niu, Y.N.; Zhao, T.; Zhang, J.Z.; Liu, Y.; Xu, Y.H.; Meng, J.; Wang, Y.C.; Wang, A.B. Chaos generation by a hybrid integrated chaotic semiconductor laser. *Chin. Phys. B* **2018**, *27*, 050502. [[CrossRef](#)]
6. Hung, Y.H.; Hwang, S.K. Photonic microwave amplification for radio-over-fiber links using period-one nonlinear dynamics of semiconductor lasers. *Opt. Lett.* **2013**, *38*, 3355–3358. [[CrossRef](#)]
7. Hwang, S.K.; Chen, H.F.; Lin, C.Y. All-optical frequency conversion using nonlinear dynamics of semiconductor lasers. *Opt. Lett.* **2009**, *34*, 812–814. [[CrossRef](#)]
8. Cui, C.; Fu, X.; Chan, S.C. Double-locked semiconductor laser for radio-over-fiber uplink transmission. *Opt. Lett.* **2009**, *34*, 3821–3823. [[CrossRef](#)]
9. Zhong, D.Z.; Luo, W.; Xu, G.L. Controllable all-optical stochastic logic gates and their delay storages based on the cascaded VCSELs with optical-injection. *Chin. Phys. B* **2016**, *25*, 094202. [[CrossRef](#)]
10. Cheng, C.H.; Lee, C.W.; Lin, T.W.; Lin, F.Y. Dual-frequency laser Doppler velocimeter for speckle noise reduction and coherence enhancement. *Opt. Express* **2012**, *20*, 20255–20265. [[CrossRef](#)]
11. Sciamanna, M.; Shore, K.A. Physics and applications of laser diode chaos. *Nat. Photonics* **2015**, *9*, 151–162. [[CrossRef](#)]
12. Li, P.; Wang, Y.C.; Wang, A.B.; Yang, L.Z.; Zhang, M.J.; Zhang, J.Z. Direct generation of all-optical random numbers from optical pulse amplitude chaos. *Opt. Express* **2012**, *20*, 4297–4308. [[CrossRef](#)]
13. Zhang, L.; Pan, B.; Chen, G.; Guo, L.; Lu, D.; Zhao, L.; Wang, W. 640-Gbit/s fast physical random number generation using a broadband chaotic semiconductor laser. *Sci. Rep.* **2017**, *7*, 45900. [[CrossRef](#)]
14. Liu, A.Y.; Zhang, C.; Norman, J.; Snyder, A.; Lubyshev, D.; Fastenau, J.M.; Liu, A.W.K.; Gossard, A.C.; Bowers, J.E. High performance continuous wave 1.3  $\mu\text{m}$  quantum dot lasers on silicon. *Appl. Phys. Lett.* **2014**, *104*, 041104. [[CrossRef](#)]
15. Liu, H.; Wang, T.; Jiang, Q.; Hogg, R.; Tutu, F.; Pozzi, F.; Seeds, A. Long-wavelength InAs/GaAs quantum-dot laser diode monolithically grown on Ge substrate. *Nat. Photonics* **2011**, *5*, 416–419. [[CrossRef](#)]
16. Chen, S.; Li, W.; Wu, J.; Jiang, Q.; Tang, M.; Shutts, S.; Elliott, S.N.; Sobiesierski, A.; Seeds, A.J.; Ross, I.; et al. Electrically pumped continuous-wave III-V quantum dot lasers on silicon. *Nat. Photonics* **2016**, *10*, 307–312. [[CrossRef](#)]
17. Sellin, R.L.; Ribbat, C.; Grundmann, M.; Ledentsov, N.N.; Bimberg, D. Close-to-ideal device characteristics of high-power InGaAs/GaAs quantum dot lasers. *Appl. Phys. Lett.* **2001**, *78*, 1207–1209. [[CrossRef](#)]
18. Capua, A.; Rozenfeld, L.; Mikhelashvili, V.; Eisenstein, G.; Kuntz, M.; Laemmlin, M.; Bimberg, D. Direct correlation between a highly damped modulation response and ultralow relative intensity noise in an InAs/GaAs quantum dot laser. *Opt. Express* **2007**, *15*, 5388–5393. [[CrossRef](#)]
19. Newell, T.; Bossert, D.; Stintz, A.; Fuchs, B.; Malloy, K.; Lester, L. Gain and linewidth enhancement factor in InAs quantum-dot laser diodes. *IEEE Photon. Technol. Lett.* **1999**, *11*, 1527–1529. [[CrossRef](#)]
20. Ukhanov, A.A.; Stintz, A.; Eliseev, P.G.; Malloy, K.J. Comparison of the carrier induced refractive index, gain, and linewidth enhancement factor in quantum dot and quantum well lasers. *Appl. Phys. Lett.* **2004**, *84*, 1058–1060. [[CrossRef](#)]
21. Shchekin, O.B.; Deppe, D.G. 1.3  $\mu\text{m}$  InAs quantum dot laser with  $T_0 = 161$  K from 0 to 80  $^\circ\text{C}$ . *Appl. Phys. Lett.* **2002**, *80*, 3277–3279. [[CrossRef](#)]
22. Markus, A.; Chen, J.X.; Paranthoën, C.; Fiore, A.; Platz, C.; Gauthier-Lafaye, O. Simultaneous two-state lasing in quantum-dot lasers. *Appl. Phys. Lett.* **2003**, *82*, 1818–1820. [[CrossRef](#)]
23. Erneux, T.; Viktorov, E.A.; Kelleher, B.; Goulding, D.; Hegarty, S.P.; Huyet, G. Optically injected quantum-dot lasers. *Opt. Lett.* **2010**, *35*, 937–939. [[CrossRef](#)]

24. Goulding, D.; Hegarty, S.P.; Rasskazov, O.; Melnik, S.; Hartnett, M.; Greene, G.; McInerney, J.G.; Rachinskii, D.; Huyet, G. Excitability in a quantum dot semiconductor laser with optical injection. *Phys. Rev. Lett.* **2007**, *98*, 153903. [[CrossRef](#)]
25. Carroll, O.; O'Driscoll, I.; Hegarty, S.P.; Huyet, G.; Houlihan, J.; Viktorov, E.A.; Mandel, P. Feedback induced instabilities in a quantum dot semiconductor laser. *Opt. Express* **2006**, *14*, 10831–10837. [[CrossRef](#)] [[PubMed](#)]
26. Viktorov, E.A.; Mandel, P.; O'Driscoll, I.; Carroll, O.; Huyet, G.; Houlihan, J.; Tanguy, Y. Low-frequency fluctuations in two-state quantum dot lasers. *Opt. Lett.* **2006**, *31*, 2302–2304. [[CrossRef](#)]
27. Olejniczak, L.; Panajotov, K.; Wiczorek, S.; Thienpont, H.; Sciamanna, M. Intrinsic gain switching in optically injected quantum dot laser lasing simultaneously from the ground and excited state. *J. Opt. Soc. Am. B* **2010**, *27*, 2416–2423. [[CrossRef](#)]
28. Viktorov, E.A.; Dubinkin, I.; Fedorov, N.; Erneux, T.; Tykalewicz, B.; Hegarty, S.P.; Huyet, G.; Goulding, D.; Kelleher, B. Injection-induced, tunable, all-optical gating in a two-state quantum dot laser. *Opt. Lett.* **2016**, *41*, 3555–3558. [[CrossRef](#)] [[PubMed](#)]
29. Tykalewicz, B.; Goulding, D.; Hegarty, S.P.; Huyet, G.; Dubinkin, I.; Fedorov, N.; Erneux, T.; Viktorov, E.A.; Kelleher, B. Optically induced hysteresis in a two-state quantum dot laser. *Opt. Lett.* **2016**, *41*, 1034–1037. [[CrossRef](#)]
30. Arsenijević, D.; Schliwa, A.; Schmeckeber, H.; Stubenrauch, M.; Spiegelberg, M.; Bimberg, D.; Mikhelashvili, V.; Eisenstein, G. Comparison of dynamic properties of ground- and excited-state emission in p-doped InAs/GaAs quantum-dot lasers. *Appl. Phys. Lett.* **2014**, *104*, 181101. [[CrossRef](#)]
31. Stevens, B.J.; Childs, D.T.D.; Shahid, H.; Hogg, R.A. Direct modulation of excited state quantum dot lasers. *Appl. Phys. Lett.* **2009**, *95*, 061101. [[CrossRef](#)]
32. Arsenijević, D.; Bimberg, D. Quantum-dot lasers for 35 Gbit/s pulse-amplitude modulation and 160 Gbit/s differential quadrature phase-shift keying. *Proc. SPIE* **2016**, *9892*, 98920S.
33. Wang, C.; Lingnau, B.; Lüdge, K.; Even, J.; Grillot, F. Enhanced dynamic performance of quantum dot semiconductor lasers operating on the excited state. *IEEE J. Quantum Electron.* **2014**, *50*, 723–731. [[CrossRef](#)]
34. Lin, L.C.; Chen, C.Y.; Huang, H.; Arsenijević, D.; Bimberg, D.; Grillot, F.; Lin, F.Y. Comparison of optical feedback dynamics of InAs/GaAs quantum-dot lasers emitting solely on ground or excited states. *Opt. Lett.* **2018**, *43*, 210–213. [[CrossRef](#)] [[PubMed](#)]
35. Huang, H.; Lin, L.C.; Chen, C.Y.; Arsenijević, D.; Bimberg, D.; Lin, F.Y.; Grillot, F. Multimode optical feedback dynamics in InAs/GaAs quantum dot lasers emitting exclusively on ground or excited states: Transition from short- to long-delay regimes. *Opt. Express* **2018**, *26*, 1743–1751. [[CrossRef](#)]
36. Yousefvand, H.R.; Faris, Z. Theoretical study of laser-mode competition in quantum-dot semiconductor lasers using a self-consistent electro-opto-thermal model. *J. Opt. Soc. Am. B Opt. Phys.* **2017**, *34*, 1580–1586. [[CrossRef](#)]
37. Wang, C.; Zhang, J.P.; Grillot, F.; Chan, S.C. Contribution of off-resonant states to the phase noise of quantum dot lasers. *Opt. Express* **2016**, *24*, 29872–29880. [[CrossRef](#)]
38. Grillot, F.; Wang, C.; Naderi, N.A.; Even, J. Modulation properties of self-injected quantum-dot semiconductor diode lasers. *IEEE J. Quantum Electron.* **2013**, *19*, 1900812. [[CrossRef](#)]
39. Ghalib, B.A.; Al-Obaidi, S.J.; Al-Khursan, A.H. Modeling of synchronization in quantum dot semiconductor lasers. *Opt. Laser Technol.* **2013**, *48*, 453–460. [[CrossRef](#)]
40. Corless, R.M.; Essex, C.; Nerenberg, M.A.H. Numerical methods can suppress chaos. *Phys. Lett. A* **1991**, *157*, 27–36. [[CrossRef](#)]
41. Butusov, D.; Karimov, A.; Tutueva, A.; Kaplun, D.; Nepomuceno, E.G. The effects of Padé numerical integration in simulation of conservative chaotic systems. *Entropy* **2019**, *21*, 362. [[CrossRef](#)]
42. Bandt, C.; Pompe, B. Permutation entropy: A natural complexity measure for time series. *Phys. Rev. Lett.* **2002**, *88*, 174102. [[CrossRef](#)]
43. Toomey, J.P.; Kane, D.M. Mapping the dynamic complexity of a semiconductor laser with optical feedback using permutation entropy. *Opt. Express* **2014**, *22*, 1713–1725. [[CrossRef](#)]
44. Osiński, M.; Buus, J. Linewidth broadening factor in semiconductor lasers-an overview. *IEEE J. Quantum Electron.* **1987**, *23*, 928. [[CrossRef](#)]

45. AL-Hosiny, N.M. Effect of linewidth enhancement factor on the stability map of optically injected distributed feedback laser. *Opt. Rev.* **2014**, *21*, 261–264. [[CrossRef](#)]
46. Heil, T.; Fischer, I.; Elsässer, W. Influence of amplitude-phase coupling on the dynamics of semiconductor lasers subject to optical feedback. *Phys. Rev. A* **1999**, *60*, 634–641. [[CrossRef](#)]



© 2019 by the authors. Licensee MDPI, Basel, Switzerland. This article is an open access article distributed under the terms and conditions of the Creative Commons Attribution (CC BY) license (<http://creativecommons.org/licenses/by/4.0/>).